Geoderma 334 (2019) 37–48

Contents lists available at ScienceDirect

Geoderma

journal homepage: www.elsevier.com/locate/geoderma

Characterizing dissolved organic matter in eroded sediments from a loess hilly catchment using fluorescence EEM-PARAFAC and UV–Visible absorption: Insights from source identification and carbon cycling

Chun Liu[a,b,c,d], Zhongwu Li[a,b,c,*], Asmeret Asefaw Berhe[d], Haibing Xiao[b], Lin Liu[b], Danyang Wang[a,c], Hao Peng[a,c], Guangming Zeng[a,c]

[a] College of Environmental Science and Engineering, Hunan University, Changsha 410082, PR China
[b] State Key Laboratory of Soil Erosion and Dryland Farming on the Loess Plateau, Institute of Soil and Water Conservation, Chinese Academy of Sciences, Yangling, Shaanxi 712100, PR China
[c] Key Laboratory of Environmental Biology and Pollution Control (Hunan University), Ministry of Education, Changsha 410082, PR China
[d] School of Natural Sciences, Life and Environmental Sciences Unit, University of California, Merced 95343, CA, USA

ARTICLE INFO

Handling Editor: A.B. McBratney

Keywords:
Soil erosion
Source fingerprinting
Fluorescence
Dissolved organic matter
Land use types

ABSTRACT

The chemical characteristics of dissolved organic matter (DOM) in soils that experience erosion and deposition are key to the biogeochemical cycle of carbon on the earth's surface. However, data related to the transport and fate of DOM from soils that experience erosion and different management practices are scarce, particularly at catchment scales. In this study, soil samples (uppermost 10 cm) were collected from uplands representing four land use types (cropland, fallow, grassland, and forests) as well as gullies, and sediment samples (100 cm sampled at 10 depths) were collected from sediments retained by a check dam. Chemical characteristics of DOM in soils and sediments, as well as subsequent source identification, were inferred from UV–Visible absorption and fluorescence excitation emission matrix (EEM)-parallel factor analysis (PARAFAC) as well as principal component analysis (PCA). The results indicated higher aromaticity, hydrophobic fraction, and molecular size in DOM from forest soils than those from other land use types and gullies. These factors were also higher in soils at the eroding sites than in sediments. EEM-PARAFAC analysis demonstrated that more protein-like components (tyrosine-like and tryptophan-like combined, accounting for > 42.77%) were present in sediments compared to soils with terrestrial humic-like substances. PCA results revealed that approximately 72% of the variance in the DOM characteristics was explained by the first two principal components and that the DOM in upland and gully soils had a negligible contribution to DOM in sediments. Combined our results indicate that, despite the large amount of sediment-associated carbon that is transported by erosion and trapped in check dams, DOM is likely mineralized during soil transport. Furthermore, biological production of new organic compounds (autochthonous sources) are likely the major source of sediment DOM in depositional settings.

1. Introduction

Dissolved organic matter (DOM) in soils is the most dynamic and bioavailable fraction of soil organic matter (SOM). DOM in natural environments is typically defined as OM that passes through a filter of 0.45 μm pore size and plays an important role in the biogeochemical cycles of carbon and other elements (in particular nitrogen) (Lal, 2003; McDowell, 2003; Battin et al., 2009). DOM can become part of the mineral-associated SOC pool by bonding to fine soil particles (Kaiser and Kalbitz, 2012). DOM is also responsible for stimulating soil microbial activity to promote the decomposition of organic matter (Kuzyakov and Cheng, 2001). Studies have shown that DOM is a heterogeneous mixture of aliphatic and aromatic polymers and its composition varies in time and space depending on proximity to sources and exposure to degradation processes (Kalbitz et al., 2003; Stedmon et al., 2003; Zsolnay, 2003; Wickland et al., 2007). DOM in inland watersheds can originate from allochthonous (e.g., plant litter and soil organic matter), autochthonous (e.g., dead bacteria, plankton, animal bodies, and macrophytes) and anthropogenic sources (e.g., effluent organic matter and manure) (Zsolnay, 2003; Lozovik et al., 2007; Derrien et al., 2017). Studies had previously suggested that source of DOM can determine its chemical properties and persistence in soils and

* Corresponding author at: College of Environmental Science and Engineering, Hunan University, Changsha 410082, PR China.
E-mail address: lizw@hnu.edu.cn (Z. Li).

https://doi.org/10.1016/j.geoderma.2018.07.029
Received 31 January 2018; Received in revised form 16 May 2018; Accepted 20 July 2018

sediments (Lal, 2003; Liu et al., 2018b). Moreover, lateral movement of sediment and water in the soil system transports some of the terrestrial DOM to rivers or reservoirs via runoff, leaching, and subsurface flow processes (McDowell, 2003). When stream water with high concentration of DOM (esp. nitrogen and phosphorus components) enters streams it can cause ecological problems, i.e., eutrophication and non-point source pollution; or be an indicator for changes in flux of C in the earth system ex. due to climate change or other environmental perturbations (Lal, 2004; Santos et al., 2016), including land degradation (Ma et al., 2014). Furthermore, improved understanding of the variables that regulate flux and dynamics of DOM between aquatic and terrestrial ecosystems is essential to determine the fate of laterally transported DOM on wide-ranging processes on the surface of the Earth (Stedmon et al., 2003; McCorkle et al., 2016).

Soil erosion, especially water erosion, connects the biogeochemical cycles of carbon in the terrestrial biosphere and the hydrosphere (Berhe et al., 2007; Assouline et al., 2017; Nie et al., 2018). Soil erosion laterally redistributes up to 5 Pg C annually in both dissolved and particulate forms of C associated with different sized mineral particles (Berhe et al., 2007; Ma et al., 2014; Wang et al., 2014). There is currently no consensus as to how much of the terrestrial carbon mobilized by soil erosion is mineralized during or after transport (Berhe et al., 2018). Some studies suggest that as low as 0 to 20% of eroded C can be mineralized during transport (Berhe et al., 2018) while others suggest that 80 to 100 % of eroded C, which is approximately 1.14 Pg C yr^{-1}, can be emitted to the atmosphere from mineralization of eroded C (Lal, 1995; Durrieu et al., 2000). Regardless of the actual amount of carbon mineralization during transport of eroded C, most of the mineralizable carbon in eroded material is expected to be associated with free particulate carbon or DOC (Lal, 2003; Ma et al., 2014). To date, although the effect of soil erosion on C dynamics (Berhe and Kleber, 2013; Li et al., 2017; Liu et al., 2018a, 2018b) and associated release of greenhouse gas are widely recognized (Lal, 2004), data related to the transport and fate of DOC in eroding systems is unavailable, particularly at catchment scale.

UV–Visible absorption and fluorescence spectroscopy have been widely applied for characterizing the optical properties of dissolved organic matter in a variety of natural environments dominated by solid particles (e.g., soil, sediment, and suspended solids) (Stedmon et al., 2003; Osburn et al., 2012; He et al., 2016), with several valuable indices for differentiating the OM from contrasting sources (Shafiquzzaman et al., 2014; Derrien et al., 2017). For example, He et al. (2016) examined the distribution behavior of sediment organic matter (SOM) between dissolved and particulate phases by comparing the spectroscopic features of pore water OM and alkaline-extractable organic matter of river sediments. Santos et al. (2016) characterized the effect of temperatures on the DOM aromaticity, mean molecular weight, organic C concentration, and major structural components by employing optical spectrophotometry. Furthermore, a series of quality indices are feasible for the sources of DOM, such as the fluorescence index (FI), humification index (HIX), biological index (BIX), and the relative abundance or the ratios of different fluorescent components, which can distinguish autochthonous, allochthonous, and anthropogenic OM (Derrien et al., 2017). Multivariate data analysis methods (e.g., principal component analysis, PCA; parallel factor analysis, PARAFAC) applied to fluorescence EEMs results have also been useful to identify the sources of the DOM in aquatic environments, and enable identification and quantification of fluorescent components in different types of samples, further enhancing the capability of source discrimination (Shafiquzzaman et al., 2014; Yang and Hur, 2014).

The Loess Plateau in the northwestern region of China, characterized by a mountainous and extremely complex topography, is an area of concern due to its high rates of soil erosion and has been intensively studied by the scientific community in recent decades (Wang et al., 2015; Li et al., 2017; Liu et al., 2017a, 2017b). Previous studies estimate that the average rate of soil loss in the Loess Plateau region is 50–100 Mg ha^{-1} $year^{-1}$, with maximum recorded rates of 200–300 Mg ha^{-1} $year^{-1}$ in some regions (Liu and Liu, 2010; Sun et al., 2014). More than 60% of the land area in this region has been subjected to soil erosion that laterally distributes essential nutrients in topsoil (including carbon, nitrogen and phosphorus) (Cai, 2001; Li et al., 2015). Approximately 0.8–1.5 kg of ammonia, 1.5 kg of total phosphorus, and 20 kg of total potassium are lost in each ton of eroded soil as estimated by Cai (2001) and 7.63 Tg C yr^{-1} of soil organic carbon is mobilized by erosion (Zhao et al., 2016). In addition to causing severe ecosystem degradation in the Loess Plateau, the high rates of soil erosion have also endangered the ecological health and security of the middle and lower reaches of the Yellow River due to high sediment load input and water eutrophication (Li et al., 2017). Consequently, the Loess Plateau region has been noted as a region with the most serious poverty and eco-environment fragility in China (Wang et al., 2011).

To control soil and water loss effectively on the Loess Plateau, a series of comprehensive biological and engineering measures were initiated by the Chinese government in 1950s. Vast areas of cropland with a slope gradient that exceeded 25° in mountainous areas were converted to forestland or grassland in the gully and hilly zones and > 90,000 check dams were constructed in gullies and streams (Zhao et al., 2016; Liu et al., 2018a, 2018b). Consequently, the intensity of soil erosion has been greatly mitigated and the sediment export to lower reaches of Yellow river has decreased significantly over the past six decades (sediment loads decreased from 1.34 ± 0.64 Gt yr^{-1} in 1951–1979 to 0.32 ± 0.24 Gt yr^{-1} in 2000–2010) (Miao et al., 2010; Wang et al., 2016). As the most widespread and effective strategy to reduce soil and water loss, check dams not only trap all of the sediments that are derived from upstream soil erosion but also intercept massive amounts of SOM in the alluvial wedges (Lü et al., 2012; Liu et al., 2017a). As estimated by Wang et al. (2011), check dams have trapped a total of 2.1×10^{10} m^3 of sediments and 0.095 Gt of organic carbon on the Loess Plateau. The depth of sediment retained by check dams have already reached several meters or tens of meters, and can be used as an important archive of the history of soil erosion and land use changes in this region (Chen et al., 2016; Liu et al., 2018b). The effect of land use type and check dam construction on SOC stocks and source identification of eroded SOM in sediment cores and during rainfall events have been reported in our previous studies in this region (Liu et al., 2017a, 2017b, 2018a). However, little information is available regarding the characteristic of DOM in the retained sediments, and how DOM characteristics in the check dams vary among land use types, gully soils, and sediments. More importantly, source identification of eroded DOM in sediments retained by check dam using spectral fingerprinting approaches is scarce.

Therefore, in order to fill this knowledge gap and as an extension of our previous studies in this region (Liu et al., 2017b, 2018a, 2018b), the main objectives of this study were: (1) to analyze differences in the structural and chemical characteristics of DOM in soils of various upland land use types and gullies by using UV–Vis absorbance and fluorescence spectroscopy; (2) to determine the characteristics of DOM in eroding and deposition soils by comparing selected spectroscopic indicators and EEM spectra; (3) to identify the primary sources of DOM in sediment cores using parallel factor analysis (PARAFAC) and principal component analysis (PCA) as a systematic approach.

2. Materials and methods

2.1. Study area

The study was conducted at a small sub-catchment (Xijiazhai watershed) (3.10 km^2) within the headstream basin of the Luoyugou watershed near Tianshui City, Gansu Province, China (105° 43′ E, 34° 36′ N), which belongs to the typical loess hilly–gully region of the Loess Plateau (Fig. 1). This region is characterized by seasonal alternations of the East Asian summer and winter monsoons, with a mean annual

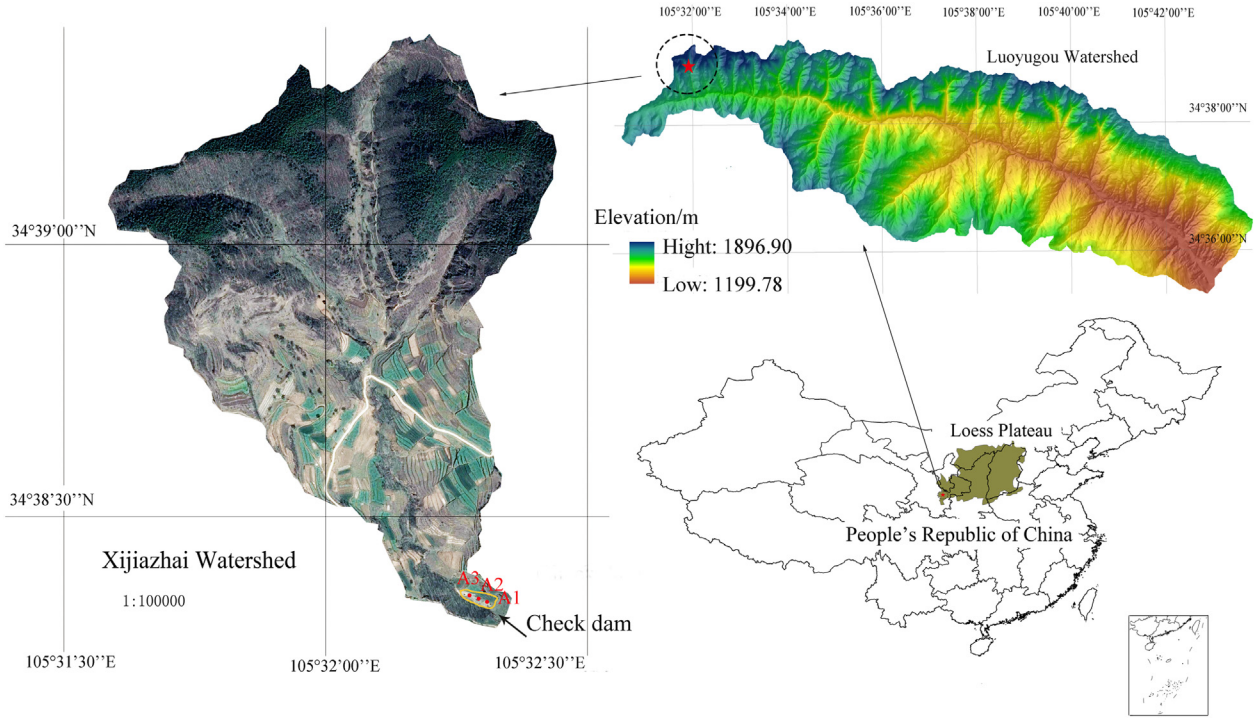

Fig. 1. Location and satellite image of studied catchment (Liu et al., 2018a, 2018b).

precipitation of 542.5 mm. The precipitation is mainly concentrated in the rainy season (from June to September), representing > 80% of the annual total, most of which occurs in the form of intense, short duration rainstorms, with large inter-annual and annual variations (Xin et al., 2016; Liu et al., 2018b). The average annual temperature is approximately 10.7 °C, with a minimum temperature of −2.3 °C in January and a maximum of 22.6 °C in July. The main soil type is dominated by Calcaric Cambisols, which are mainly covered by agricultural land, followed by Haplic Greyzems and then Calcaric Fluvisols, which mainly appear in highland and valley areas, respectively, according to the recent soil classification system of FAO (2014). The soils in this region have primarily developed from loess parent materials and have a silty loam texture. Soil erosion in the basin is given priority to hydraulic erosion and gravity erosion (Liu et al., 2017b, 2018b).

In this catchment, several soil and water conservation measures were carried out starting in the 1950s. The control practices mainly included grazing exclusion, constructing check dams, terrace building, grass planting, and afforestation, as shown in Fig. 1. In addition, a road was constructed in the middle part of catchment to connect nearby villages. The primary land uses in this area are forest and cropland. The majority of forests are in steep areas, whereas croplands are located in relatively level areas, and only small areas are composed of grassland and abandoned land (Fig. 1). A dry main stream and four tributaries occur in gullies and the flow direction is from north to south. A sediment-trapping reservoir (i.e., check dam) was constructed at the outlet of this catchment, and large amounts of sediments were retained, with the depth of 1 m since 2004. The land use and check dam construction history, along with the deposition depth of sediment were reconstructed from interviews with farmers and a field campaign in 2016.

In this catchment, almost all the land use was cropland except in areas with steep slopes where crops could not be grown. No fallow land existed in the catchment before 1990. Ecological forest construction was initially implemented in the 1950s and was expanded beginning in 2002 as part of the Grain for Green Project, which converted sloping croplands to forests, grasslands, and fallow land in this region (Xin et al., 2016). As a result, the current primary landscape units are cropland and forests, and the total area of grassland, fallow and gullies relative to the total catchment area is small.

2.2. Sample collection and preparation

2.2.1. Source material sampling at eroding sites

A detailed description of SOM sampling was provided in our previous studies (Liu et al., 2018a, 2018b). In brief, source material sampling involved the collection of surface soils (0–10 cm) from eroding areas that represent each of the uncultivated (e.g., forest (FS), grassland (GL), fallow land (FL), and gully (GY)) and cultivated (cropland (CL)) sites. Soil sampling sites were selected on the basis of topography and slope positions (upper, middle, lower) under different land use types and along the stream in the small catchment after field direct investigations and discussions with catchment staff and land-owner. In total, 72 samples of surface soils were collected between July and August 2016: 18 samples from gullies, 9 samples from fallow land, 18 samples from cropland, 18 samples from forests, and 9 samples from grassland. For each sampling site, 5 sub-samples were collected from 0 to 10 cm depth along transects at a 5 × 5 m grid and combined in the field to form a composite sample. Samples from channel banks were collected along the trench wall. Three samples were composited for analysis, one near the base of the bank, one near the middle of the bank and the other near the top of the bank. Meanwhile, gullies were sampled from different positions near the channel bank to collect surface sediment composite samples downstream. Channel bank and gully samples were taken using a 7.0 cm-diameter soil sampler to a 10 cm depth.

Furthermore, aspects, gradients, and altitudes were recorded in situ at each quadrat using a global positioning system receiver (GPS), with an accuracy of approximately 1 m. The soil cores were collected in situ using 100 cm^3 volume stainless steel tubes for the measurement of soil bulk density (BD) and soil moisture content (SMC) with three replicates at each sampling site. All undisturbed samples were taken with three replicates to reduce experimental errors in this study (Liu et al., 2018a, 2018b).

2.2.2. Sediment sampling at depositional sites

Sediment sampling was performed from head to tail along the check dam. Three sediment profiles (A1, A2, and A3) were dug with picks and spades behind the check dam, as described in previous works from the same study area (Liu et al., 2018b). Sediment samples (0–100 cm deep) were taken from each sediment profile with the 10 cm intervals based on the sedimentation history. A total of 90 bulk samples (10 depths, 3 profiles, and 3 replications) were collected using a 7.0 cm-diameter soil sampler for the physio-chemical properties and spectrum analysis. Meanwhile, soil cores (100 cm^3 volume stainless steel tubes) were also collected with three replicates at each sampling site for the measurement of soil BD and SMC (Liu et al., 2018a, 2018b).

2.3. Laboratory analysis

All soil and sediment samples were packed in polyethylene plastic bags and transported on ice to the laboratory as soon as possible. All samples were freeze-dried, ground slightly, and passed through a 2-mm mesh sieve to remove coarse fragments and litters prior to further analysis. The soil pH was determined with a soil–water ratio of 1:2.5 using HI 3221 pH meter (Hanna Instruments Inc., USA) (Li et al., 2017). The soil texture and specific surface area (SSA) were analyzed using a Laser Particle Size Analyzer (Mastersizer 2000, Marlven, Ltd. UK). The measurements spanned sizes from 0.02 to 2000 μm (Liu et al., 2017a, 2017b). Bulk samples were dried at 105 °C for 48 h in the oven. The soil BD was calculated by dividing the oven-dried soil mass by the steel cylinder volume and the SMC was determined gravimetrically by oven drying the whole soil sample to calculate the dry soil bulk density (Carter, 1993).

The soil-derived DOM was extracted by using milli-Q water with a DI water to soil ratio of 5:1 (v/w) in 150 cm^3 Erlenmeyer flasks on a reciprocating shaker at a speed of 250 rpm, with a shaking time of 12 h at a temperature of 25 °C. After shaking, the extracts were centrifuged at 3500 rpm for 25 min, and the supernatants were filtered through a 0.45-μm cellulose acetate membrane filter before the analysis. All extracts were stored in sterilized amber glass vials at 4 °C before further analysis. DOC concentration was measured by using a Shimadzu TOC-VCPH (Shimadzu Corp., Kyoto, Japan) via the combustion oxidation nondispersive infrared absorption method with a long term precision of < 3% (Yang and Hur, 2014; He et al., 2016).

Prior to the UV and fluorescence measurements, DOC concentrations of all samples were diluted to 10 mg L^{-1} with de-ionized water to get an absorbance > 0.05, as suggested to minimize the inner filtering influences (Ohno, 2002; He et al., 2016; Huang et al., 2018). The UV–Visible absorbance spectra on each extracted sample were performed by using a UV–Vis spectrometer (Shimadzu UV2000) from λ = 200 to 800 nm and using Millipore water as blank with 1 cm quartz cuvette (Shafiquzzaman et al., 2014). The specific UV absorbance at 254 nm ($SUVA_{254}$) and at 260 nm ($SUVA_{260}$) were determined by dividing the UV absorbance measured at λ = 254 nm and λ = 260 nm by the sample's DOC concentration (mg·C·L^{-1}) as an indicator of aromaticity and hydrophobic fraction of DOM, respectively, expressed as L mg C^{-1} m^{-1} (Dilling and Kaiser, 2002; Weishaar et al., 2003). The ratio of absorption at 250 nm to 365 nm (a250:a365) was calculated as a proxy of the aromaticity and the average molecular weight of DOM (Peuravuori and Pihlaja, 1997).

Fluorescence measurements were conducted using a spectro-fluorometer (Shimadzu F-7000, Hitachi) equipped with a 150 W xenon lamp at an ambient temperature of 24 °C. A 1 cm quartz cuvette with four optical windows was used for the analysis. Emission scans were performed from 250 to 600 nm at 5 nm steps, with excitation wavelengths from 200 to 500 nm at 5-nm increments. The detector was set to high sensitivity, and the scanning speed was maintained at 2400 nm/min in this study (Shafiquzzaman et al., 2014). According to an inter-laboratory standard method proposed by Murphy et al. (2010), the EEM data was corrected with a water blank. Prior to analysis, the Raman and Rayleigh scatters were removed according to the protocol of Bahram et al. (2006). EEMs were converted to Raman units (R.U.) using the area under the Milli-Q Raman scatter peak with an excitation wavelength of 350 nm and emission wavelengths from 365 to 430 nm (Lawaetz and Stedmon, 2009).

The humification index (HIX) was estimated by the ratio of the area under the fluorescence emission spectra at the wavelengths from 435 to 480 nm to that from 300 to 345 nm using an excitation wavelength of 254 nm (Zsolnay et al., 1999). The fluorescence index (FI) was the ratio of the emission intensity at 450 nm to that at 500 nm using an excitation wavelength of 370 nm, which has been long considered as an index for differentiating between terrestrial and microbial DOM (~1.9 for microbial fulvic acid and ~1.4 for terrestrial fulvic acids) (McKnight et al., 2001). The biological index (BIX) was calculated as the ratio of the fluorescence intensity at emission 380 nm to that at 430 nm for an excitation wavelength of 310 nm, which corresponded to 0.6–0.7 for DOM of low autochthonous component and > 1 for DOM of biological or aquatic bacterial origin (Huguet et al., 2009). PARAFAC modeling was performed based on a total of 172 EEMs of soil and sediment OM using the DOMFluor toolbox in MATLAB 2015a (Math-works, Natick, MA) (Stedmon and Bro, 2008). PARAFAC was computed using two to seven component models with non-negativity constraints, and then residual analysis, split-half analysis, and visual inspection were applied to determine the number of fluorescence components (Huang et al., 2018). The normalized concentration in Raman unit (RU) and the percent abundance of each PARAFAC component were estimated based on the maximum fluorescence Intensity (F_{max}) output from DOMFluor (Yang et al., 2015). More detailed information of PARAFAC analysis has been described elsewhere (Bro, 1997; Stedmon and Bro, 2008; Yang et al., 2015).

2.4. Statistical analysis and modeling

All statistical tests were carried out using SPSS version 18.0 (SPSS Inc., Chicago, IL, USA). The mean ± standard deviation of physio-chemical properties (BD, SMC, pH, and soil grain size), DOC, and proxies of DOM were conducted. Significant differences were evaluated among potential sources and sediment at depths via using one-way analysis of variance (ANOVA) and least significant differences (LSD). Fitting of spectral slope and integral area was carried out using Origin 8.0. In order to identify the relative impacts from terrestrial sources (i.e., FS, GL, FL, GY, and CL) on the eroded DOM in sediments retained by the check dam, principle components analysis (PCA) was also utilized in a qualitative manner. PCA is an excellent statistical tool for handling multivariate data with minimum loss of the information (Nguyen and Hur, 2011; Shafiquzzaman et al., 2014). An aggregate of seven parameters of all soil and sediment samples was incorporated into the PCA, including both SUVA, humic-like component (HLC), a250:a365, FI, HIX, and BIX.

3. Results and discussion

3.1. DOC characteristics of soils and sediments

The DOC concentration was highest in forest soils (mean 30.23 ± 2.57 mg L^{-1}) and lowest in gullies (mean 6.90 ± 1.42 mg L^{-1}). A significant difference in DOC concentration was found between forests and other soil samples (P < 0.05) (Table 1). This may be due to differences in the amount and forms of organic material added to soil under different vegetation types, as well as the higher sequestration of DOC after landuse change from farming land to forestland and abandoned land (Chantigny, 2003; Li et al., 2017; Szymański, 2017).

The DOC concentration in each profile of sediments trapped by the check dam is presented in Fig. 2. The three soil profiles were distributed along the check dam from upstream (core A3) to downstream (core A1).

Table 1
Bulk parameters of potential sources in the watershed.

Sampling sites	DOC concentration (g kg^{-1})	Bulk density (Mg m^{-3})	Soil moisture content (%)	pH	Soil texture (%)		
					Clay	Silt	Sand
Forests	30.23 ± 2.57^{a}	1.35 ± 0.15^{a}	9.74 ± 2.98^{b}	7.90 ± 0.39^{c}	17.62 ± 4.05^{b}	35.34 ± 5.94^{b}	47.04 ± 9.40^{a}
Grassland	12.39 ± 1.98^{b}	1.41 ± 0.13^{a}	7.42 ± 1.76^{b}	8.16 ± 0.30^{ab}	25.33 ± 3.87^{a}	44.99 ± 6.98^{a}	29.68 ± 10.46^{b}
Cropland	11.94 ± 1.09^{b}	1.16 ± 0.11^{b}	10.52 ± 8.56^{b}	8.10 ± 0.12^{bc}	22.76 ± 2.43^{ab}	42.12 ± 1.86^{a}	35.12 ± 3.47^{b}
Fallow	10.08 ± 0.64^{b}	1.34 ± 0.06^{a}	9.23 ± 1.68^{b}	8.33 ± 0.07^{a}	24.39 ± 1.69^{ab}	43.87 ± 3.15^{a}	31.74 ± 2.62^{b}
Gully	6.90 ± 1.42^{b}	1.35 ± 0.13^{a}	22.56 ± 9.51^{a}	8.32 ± 0.18^{a}	26.83 ± 7.56^{ab}	39.22 ± 4.43^{ab}	33.95 ± 10.24^{b}

Note: The values represented as mean values ± standard deviation. DOC, dissolved organic carbon. Different letters (a, b, and c) indicate significant differences among various land use types and gully at $P < 0.05$.

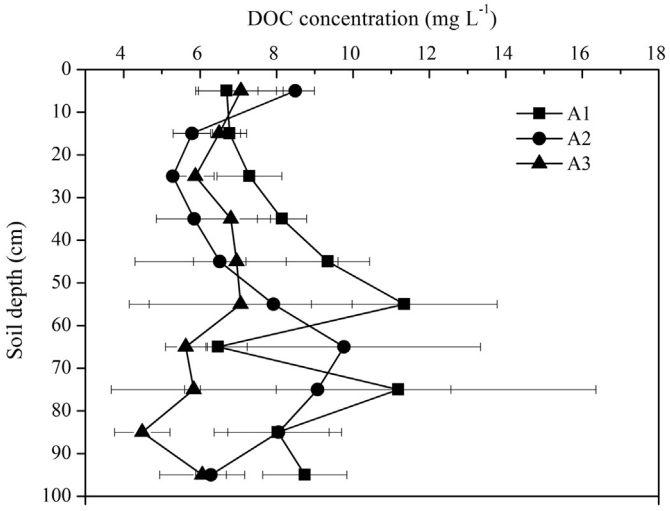

Fig. 2. Vertical distribution of dissolved organic carbon concentration in sediments at depositional site (n = 90).

The DOC concentration varied from 4.49 to 7.07 mg L^{-1} in the upstream profile, from 5.29 to 9.76 mg L^{-1} in the midstream profile, and from 6.47 to 11.34 mg L^{-1} in the downstream profile. A significant difference in DOC concentration was found between upstream (average value: 6.23 ± 0.26 mg L^{-1}) and downstream profiles (average value: 8.40 ± 0.56 mg L^{-1}) ($P < 0.05$). The difference may due to variations in hydrodynamic conditions along the flow pathway (Chen et al., 2016). The concentration of DOC in sediments was similar to that in gully soils and lower than other land use types, indicating that some of the DOC transported to sediments may have been mineralized during soil detachment, transport and deposition processes (Lal, 2003). Based on Pearson correlation analysis, the DOC concentration in sediments at depositional sites showed a highly significant positive correlation with SMC as well as silt, and a negative correlation with BD, pH, and sand ($P < 0.01$) (Table 2). However, the DOC content in soils at eroding sites was negatively correlated with pH ($P < 0.05$) and had a highly significant negative correlation with silt and clay and a positive correlation with sand ($P < 0.01$). Surprisingly, no significant correlation was found among DOC, BD, and SMC in soils at eroding sites (Table 2). The results indicated that the difference in major factors affecting DOC dynamics could lead to differences in DOC concentrations between eroding and deposition sites (Liu et al., 2017a, 2018b).

3.2. UV–vis absorbance of DOM in soils and sediments

$SUVA_{254}$, an index of aromatic structures in DOM, is widely used to identify OM originating from soils, sediments, or aquatic ecosystems (Yang et al., 2015; He et al., 2016). The DOM samples extracted from soils at the eroding sites showed a range of $SUVA_{254}$ values from 4.86 ± 0.47 to 6.29 ± 2.00 L mg C^{-1} m^{-1}, with forests soils having the highest values and fallow soils having the lowest values (Fig. 3). The values of $SUVA_{254}$ were significantly higher than those in various aquatic ecosystems (Nguyen and Hur, 2011; He et al., 2016), indicating that the soil DOM in terrestrial systems contains relatively higher aromatic fractions. The reason might be explained by the higher likelihood of biogeochemical transformations of aromatic substances via photochemical processes and microbial activities in aquatic environments compared with terrestrial environments (Wickland et al., 2007; Yang and Hur, 2014). At the eroding sites, no significant difference was found among different land use types and gullies, except for between forests and fallow (Fig. 3). This may be due to the common constituents of vascular plant-derived DOM, particularly aromatic-enriched components, which may remain unchanged after biodegradation processes in this region (Wieder et al., 2008).

The values of $SUVA_{260}$ among the soil samples were similar to those of $SUVA_{254}$, exhibiting the highest absorbance in forests and the lowest in fallow. However, the ratios of a250:a365 displayed an opposite trend among the soil samples, where the forests were lowest and fallow highest. This implies that soils in forests had higher aromaticity, hydrophobic fraction and molecular size in DOM than soils in other land uses and gullies (Peuravuori and Pihlaja, 1997; Weishaar et al., 2003; Shafiquzzaman et al., 2014).

The mean $SUVA_{254}$ values of sediments varied between 3.36 and 4.70 mg C^{-1} m^{-1}, with a mean value of 3.84 ± 0.85 L mg C^{-1} m^{-1} in the entire sediment profile. The $SUVA_{254}$ values showed a slight declining trend with increasing depth, except in the 30–40 cm layer (Fig. 4). The values of $SUVA_{254}$ in sediments at the depositional sites were lower than those of soils at the eroding sites. The values of $SUVA_{260}$ were similar to those of $SUVA_{254}$ and showed the same variation trends with depth with a range from 3.07 to 4.35 (Fig. 4). The ratio of a250:a365 showed significant variation at the surficial layer (0–30 cm) and then tended toward a stable value with depth except for

Table 2
Pearson correlation coefficients between DOC concentration and physico-chemical variables at the eroding and depositional sites.

Locations		BD	SMC	pH	Sand	Silt	Clay
Eroding site	DOC	0.077	−0.039	−0.384^{a}	0.526^{b}	−0.478^{b}	−0.529^{b}
Depositional site	DOC	−0.407^{b}	0.414^{b}	−0.278^{b}	−0.511^{b}	0.627^{b}	0.250^{a}

Notes: DOC, dissolved organic carbon; BD, bulk density; SMC, soil moisture content.
[a] Correlation is significant at the 0.05 level (2-tailed).
[b] Correlation is significant at the 0.01 level (2-tailed).

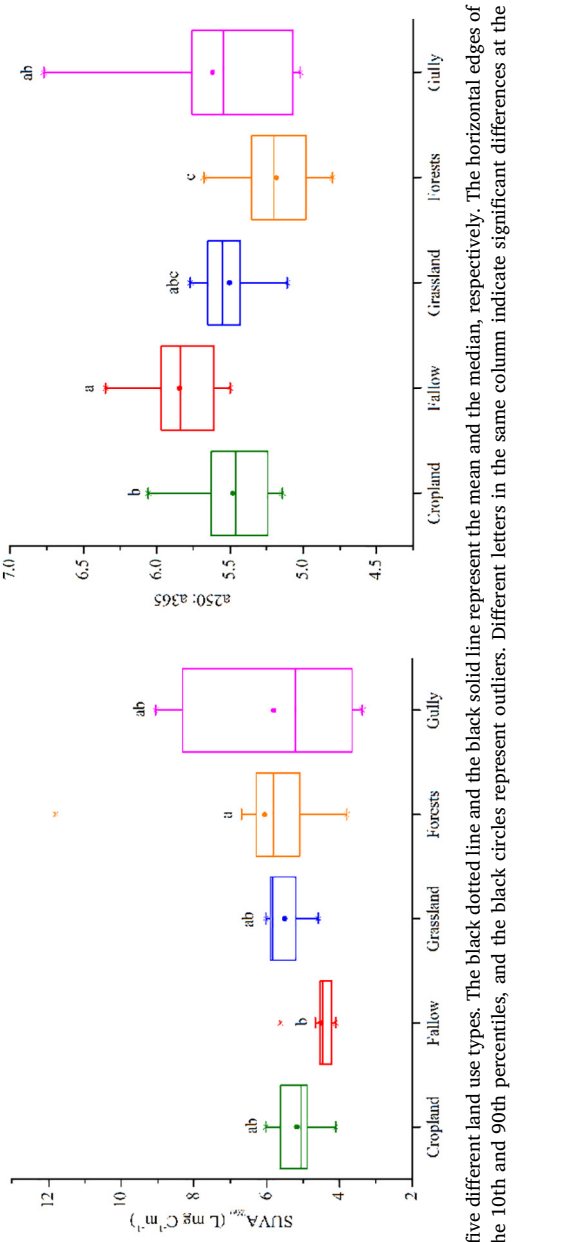

Fig. 3. Box plots of SUVA254, SUVA260, and a250:a365 for the soils of five different land use types. The black dotted line and the black solid line represent the mean and the median, respectively. The horizontal edges of the boxes denote the 25th and 75th percentiles, the whiskers denote the 10th and 90th percentiles, and the black circles represent outliers. Different letters in the same column indicate significant differences at the $P < 0.05$ level based on one-way ANOVA.

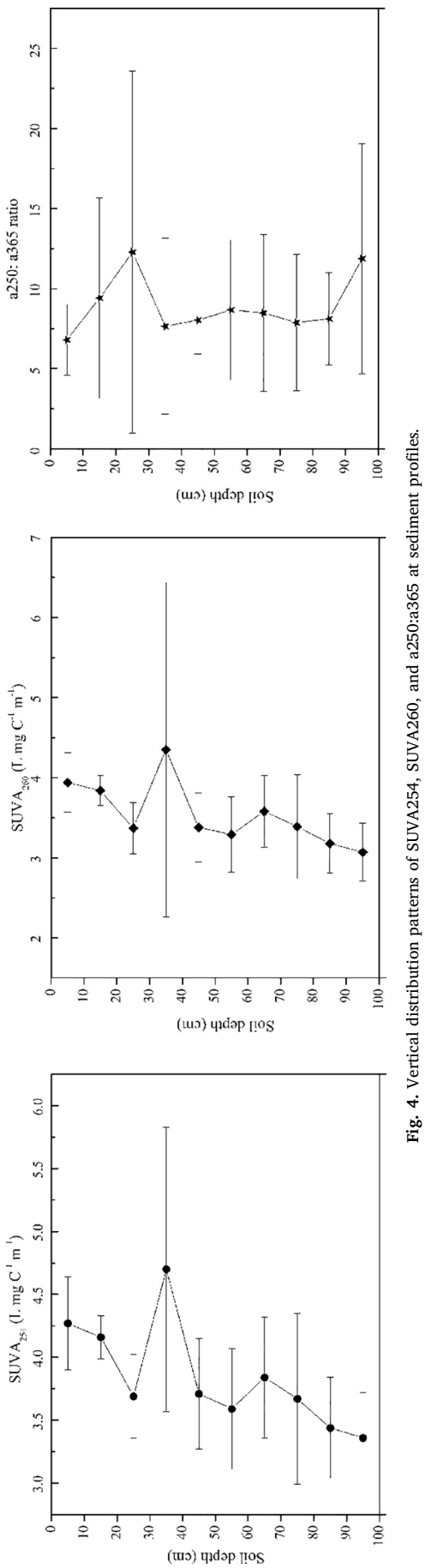

Fig. 4. Vertical distribution patterns of SUVA254, SUVA260, and a250:a365 at sediment profiles.

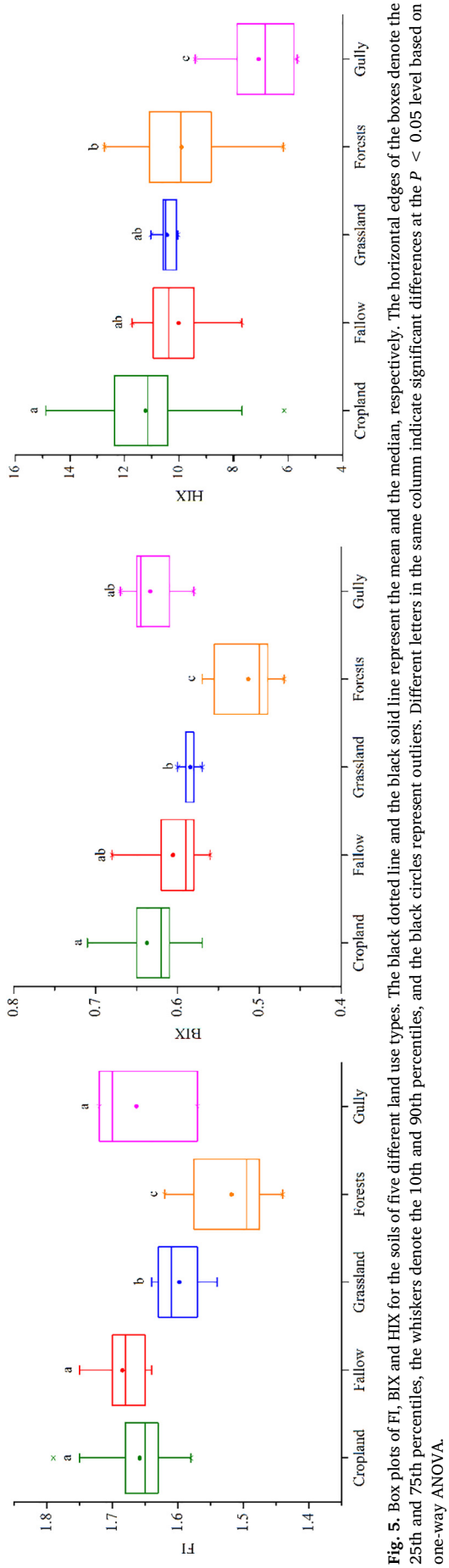

Fig. 5. Box plots of FI, BIX and HIX for the soils of five different land use types. The black dotted line and the black solid line represent the mean and the median, respectively. The horizontal edges of the boxes denote the 25th and 75th percentiles, the whiskers denote the 10th and 90th percentiles, and the black circles represent outliers. Different letters in the same column indicate significant differences at the $P < 0.05$ level based on one-way ANOVA.

an increase at the bottom layer. The values of a250:a365 in the sediment profile were higher those of soils under different land use types and gullies (Fig. 4). The results indicated that compared with soils at the eroding site, sediments at the deposition sites have less aromaticity, hydrophobic fraction, and molecular size in DOM (Derrien et al., 2017). Our study was consistent with a previous study reported by Fissore et al. (2017), showing greater presence of aromatics at eroding sites than at depositional sites likely due to the contribution of eroded upslope materials for a hillslope system in Southern California. Alternatively, the results could also suggest input of large amounts of fresh OM that is depleted in aromatic components in the depositional settings (Berhe et al., 2008, 2012; Berhe and Kleber, 2013).

3.3. Fluorescence characteristics of soils and sediments

The fluorescence index (FI) has been utilized to differentiate between terrestrial and microbial DOM sources. In general, FI values higher than 1.55 are associated with microbial-derived DOM sources (Cory et al., 2010; McKnight et al., 2001). The FI values of our soil samples exhibited a range between 1.44 and 1.79 with the highest value shown for fallow (Fig. 5). The values of FI in soils were higher than the typical values expected from the terrestrial sources (1.4) and lower compared to the values from microbial sources (1.9) (McKnight et al., 2001). The results indicated that microbial transformation in DOM may have altered the FI values and that eroding sites contained a mixture of DOM sources (Nguyen and Hur, 2011). Significant correlations in FI values were found between grassland, forests and other sources. However, no significant difference was observed among cropland, fallow, and gully (Fig. 5).

No significant difference in BIX was found among land use types and gullies, except for forests where a correlation with other sources was found ($P < 0.05$) (Fig. 5). The values of BIX ranged from 0.52 in forests to 0.64 in cropland, with a mean value of 0.60 in this region, implying that there was low biological activity in soil samples (Yang and Hur, 2014; He et al., 2016). A large variation in the values of HIX was observed among the soil samples, ranging from 5.67 to 14.88. HIX had the highest values in cropland (11.22 ± 2.14) and the lowest values in gullies (7.06 ± 1.40). A significant correlation relationship among forests, gully and cropland was found, and no significant correlations among cropland, fallow and grassland were found in this study.

The FI values of sediment samples showed little variation with increasing depth at depositional sites, ranging from 1.70 to 1.76 with an average value of 1.74 at the sediment profile. The values of IF in sediments were slightly higher than all soil samples at the eroding sites. No significant difference in the FI values was found between the surface layer (1.71 in 0–20 cm deep) and deeper layer (1.74 in 20–100 cm deep) ($P > 0.05$) (Fig. 6). This may be because the extent and the direction of the microbial change in FI values may differ by DOM sources (Hur, 2011). These FI values suggest that DOM in the depositional sites reflects some mixing of terrestrial and microbial sources (McKnight et al., 2001). BIX and FI had similar trends in the sediment profiles, with the values of BIX ranging between 0.66 and 0.73. These results suggest allochthonous sources are the major sources of DOM in sediments retained by check dam (Fig. 6) (Huguet et al., 2009). The values of HIX in sediments at depositional sittings showed no regular variation as depth increased, with a reduction in the surface layer (0–30 cm deep) and then increase in fluctuation in the deeper layer (30–100 cm deep). The HIX values in sediments were lower than those of soils in land use types and gullies, ranging from 4.85 to 6.71 (Fig. 6). These results indicate that the sediments retained by check dams contain lower amounts of condensed polyaromatic structures and higher amounts of oxygen-containing functional groups compared to soils at the eroding sites (Fuentes et al., 2006), which may be partially affected by additional DOM sources and biogeochemical processes other than microbial degradation (Nguyen and Hur, 2011). Moreover, in the sediment profile the surface layer had a higher degree of humification than the deep

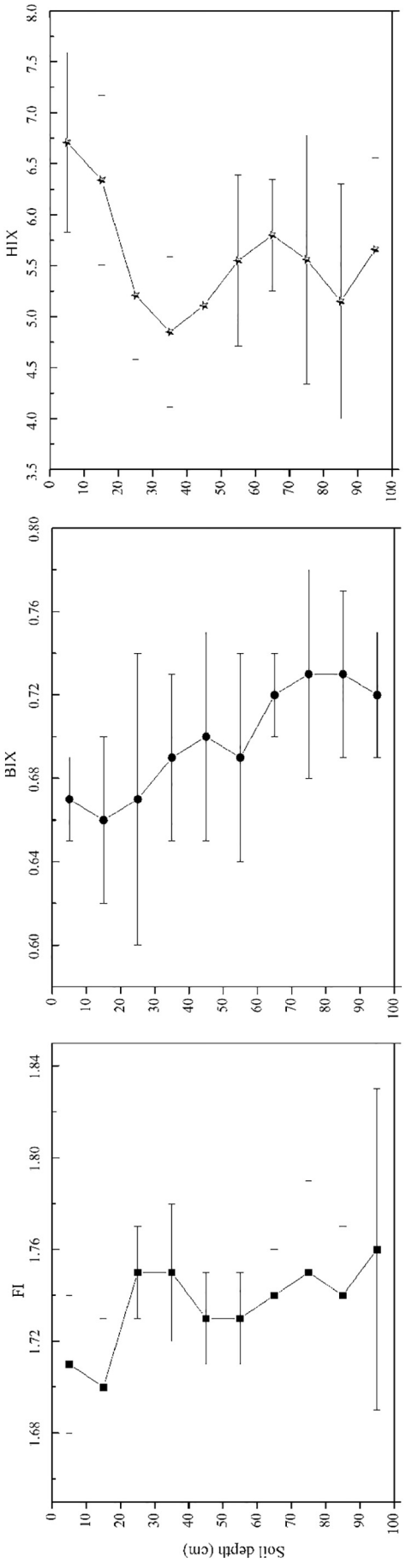

Fig. 6. Vertical distribution patterns of FI, BIX, and HIX at sediment profiles.

layer (Zsolnay et al., 1999).

3.4. Distribution of EEM components between soils and sediments using PARAFAC analysis

Typical EEM components of soils and sediments are shown in Fig. 7. Three and four components were extracted from the EEM dataset in soil OM and sediment OM using PARAFAC analysis, respectively. Based on previous studies and compared with those in the OpenFluor database, three components (C1, C2, and C3) in all soil samples in our study could be classified as humic-like substances (Coble, 1996; Stedmon et al., 2003; He et al., 2016; Huang et al., 2018) (Fig. 7a). C1 (Ex/Em = 270/460) could be classified as traditional humic-like peak C (Coble et al., 1998). As for C2 (Ex/Em = 250/400), its fluorescence peaks resembled a traditional humic-like peak A (Coble et al., 1998; Coble, 2007). C3 (Ex/Em = 220/426) was also classified as a humic-like substance (Stedmon et al., 2003). Peak A represents poly-aromatic humic acid (PAHA), whereas peak C represents poly-carboxylate humic acid (PCHA), which is typically derived from the breakdown of plant and animal substances (Lee et al., 2008).

Sediment OM had more peaks compared to soil OM, with an additional EEM peak shown at the Ex/Em wavelengths of 230 (280)/346 nm and 200/300 nm. Four components were extracted from the EEM dataset and compared with those in the OpenFluor database (Murphy et al., 2014) (Fig. 7b). C1 had Ex/Em maximum wavelengths at 240/412 nm, which can be assigned to a terrestrial humic-like component (Stedmon et al., 2003); Component C2 had Ex/Em maximum wavelengths at 270 (370)/460 nm, which was similar to UVC + UVA humic-like fluorophore (Coble, 1996; Stedmon et al., 2003); The third PARAFAC component, C3, with the Ex/Em wavelengths of 230 (280)/346 nm was assigned to the tryptophan-like peak T at Ex/Em (225, 275)/340 nm (Coble, 1996, 2007); C4, with the Ex/Em wavelengths of 200/300 (420) nm was similar to the tyrosine-like fluorophore, but it also had the source from other humic-like fluorophore, such as the microbial humic-like component (Coble, 2007; Chen et al., 2015). Aside from the terrestrial humic-like substance, the protein-like components C3 and C4 (tyrosine-like and tryptophan-like combined) detected in sediments retained by check dams indicated that biological production of organic compounds from autochthonous sources may be the primary source of sediment organic matter in the deposition sites, rather than soil organic matter input induced by erosion upstream from allochthonous sources.

3.5. Identification of sediment DOM sources using principal component analysis

In order to further analyze the contribution to DOM in sediments at deposition sites from terrestrial sources, PCA was used to qualitatively identify the primary source of eroded DOM in sediments from five possible sources at the eroding sites (e.g., CL, AL, FL, FS, and GY). 7 parameters were used as variables for the PCA: FI, HIX, BIX, $SUVA_{254}$, $SUVA_{260}$, a250:a365, and HLC. These parameters were selected based on the wide range of values among the different soil and sediment samples so that each DOM source could be easily distinguished by the values (Nguyen and Hur, 2011). The factor loadings, Eigen-values and variance percentage corresponding to each principal component are presented in Table 3. The first two principal components (PC1 and PC2) explained over 72% of the total data variance. PC1 was responsible for 55.21% of the variance and highly positively correlated with HIX, both SUVA values, and HLC. PC1 was negatively correlated with FI and BIX (Table 3 and Fig. 8a). Based on the sign and the contribution of measured parameters, PC1 can be interpreted as a factor associated with humic-like aromatic compounds, condensed polyaromatic structures and enrichment of proteins in the samples (Nguyen and Hur, 2011; Shafiquzzaman et al., 2014). PC2 explained 16.91% of the total variance and exhibited strong negative loading for a250:a365 (Table 3 and

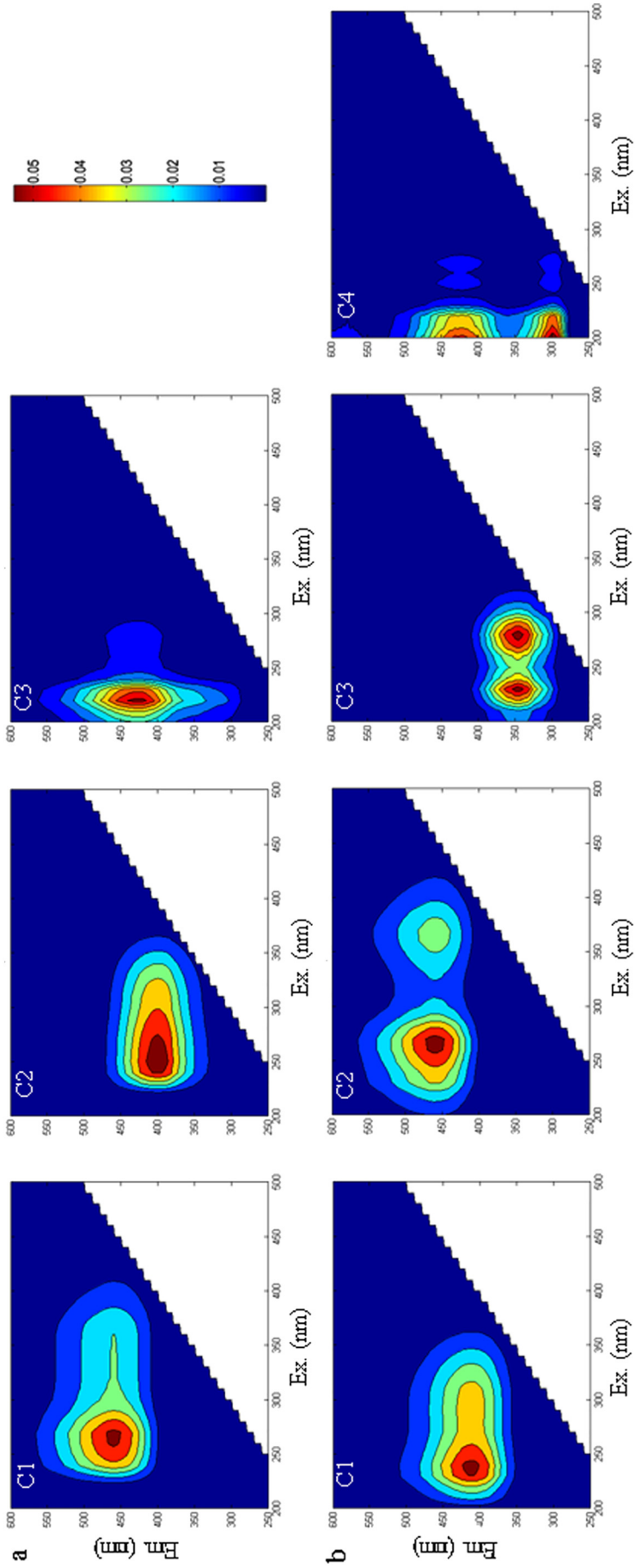

Fig. 7. Contour plots of EEM-PARAFAC components of DOM in soils (a) and sediments (b). C1, C2, and C3 in section a represent humic-like substances with a combination of UVC humic-like peak A and UVA humic-like peak C; C1, C2, C3, and C4 in section b represent terrestrial humic-like components, UVC + UVA humic-like fluorophore, tryptophan-like, and tyrosine-like fluorophore, respectively. Color indicates the degree of the fluorescence intensity under the excitation and emission wavelengths.

Table 3
Eigenvalues and variance percentages corresponding to the principal component (PC). Value with bold indicated strong factor loading.

	PC1	PC2
SUVA254	**0.894**	0.043
SUVA260	**0.891**	0.049
a250:a365	−0.405	−0.669
SR	−0.129	**0.907**
HIX	**0.852**	−0.019
FI	−0.795	−0.0.132
BIX	−0.793	−0.228
HIC	**0.811**	0.100
Eigenvalue	4.525	1.245
Variability (%)	55.205	16.913
Cumulative %	55.205	72.118

Fig. 8a), indicating higher aromatic humic-like matter with a high molecular weight related to terrestrial inputs such as agriculture runoff, snow melt, soil, peat, etc. (Fernando et al., 2007; Shafiquzzaman et al., 2014).

The score plot of different sources and sediments is shown in Fig. 8b. From the score plot, FS and GL showed highly positive scores on the PC1 axis, which indicated that these sources were associated with the presence of proteins and amino acids (Shafiquzzaman et al., 2014). In contrast, the sediment samples (L1: 0–10 cm; L2: 10–20 cm; L3: 20–30 cm; L4: 30–40 cm; L5: 40–50 cm; L6: 50–60 cm; L7: 60–70 cm; L8: 70–80 cm; L9: 80–90 cm; L10: 90–100 cm deep) exhibited negative loadings in PC1. Based on the score plot, the properties of the DOM sources in all soils (including CL, FS, FL, GL, and GY) appeared to be different from all sediment samples. All soil samples exhibited moderate positive loading on PC1 and all sediment samples displayed moderate negative loadings on PC1. This implied that the DOM in soils made a negligible contribution to DOM in sediments retained by check dam.

Combined results demonstrated that the properties of the DOM in sediments were primarily drived by autochthonous sources, not allochthonous sources in this study. This is likely due to the decomposition and mineralization of DOM by microbial activity during soil detachment, transport and deposition processes induced by erosion (Lal, 2003, 2004). Previous studies have also indicated that the solubility characteristics of SOC could also drive high C loss associated with high surface runoff and soil loss during rainfall events (Jacinthe et al., 2002; Jin et al., 2008; Ma et al., 2014).

3.6. Implications for future studies

In this study, the characteristic and fate of DOC in erosion and depositional processes was explored at the catchment scale using EEMs-PARAFAC modeling and spectral indices. The results are relevant to balancing the regional carbon budget, ascertaining the role of DOC dynamics in the global carbon cycle, and informing the sink/source controversy of C redistribution induced by soil erosion from an eco-geomorphologic perspective (Kirkels et al., 2014; Liu et al., 2018a). Because the dynamics of the SOC pool are complex and heterogeneous, assessing the impacts of soil erosion, transport and deposition processes under different management practices on lateral and vertical SOC fluxes still presents a challenge (Smith et al., 2001; Doetterl et al., 2012). Gaps remain on our understanding of variables that control SOM flux and composition in dynamic landscapes as there are very few long term monitoring studies that have included advanced analytical and modelling studies to determine broad scale spatio-temporal dynamics SOC over the Earth's land surface (Kirkels et al., 2014). Furthermore, although the spectroscopic indices (absorption-and fluorescence-based indices) are feasible and useful for characterizing OM and identifying sources of OM, they also have limitations that can raise challenges for their use and interpretation (Derrien et al., 2017). On the one hand, biogeochemical transformations including photochemical processes and microbial activities after mixing of multiple sources exert further effects on the optical properties of OM (Helms et al., 2008; Zhou et al., 2017); on the other hand, the spectroscopic indices are sensitive to solution chemistry (e.g., pH, OM concentration, and the complexated metals), and constrained to the colored and fluorescent components of organic matter without relationships with bulk DOM (Yang and Hur, 2014; Derrien et al., 2017). Therefore, it remains difficult to carry out such studies on how biogeochemical processes reflect spectroscopic indices and explicate the role of differences in quantity of microbes and microbial community composition on DOC dynamics over three landscape domains: eroding sites, the transport pathway along hillslopes, and depositional sites within terrestrial ecosystems (Eilers et al., 2012; Derrien et al., 2017).

4. Conclusions

In this study, the nature of DOM in soils of different land use types and sediments in a check dam was explored by using selected spectral indicators and EEM-PARAFAC components. DOM of soils in forests had higher aromaticity, hydrophobic fraction, and molecular size than that of soils in other land uses and gullies, indicating high concentration of

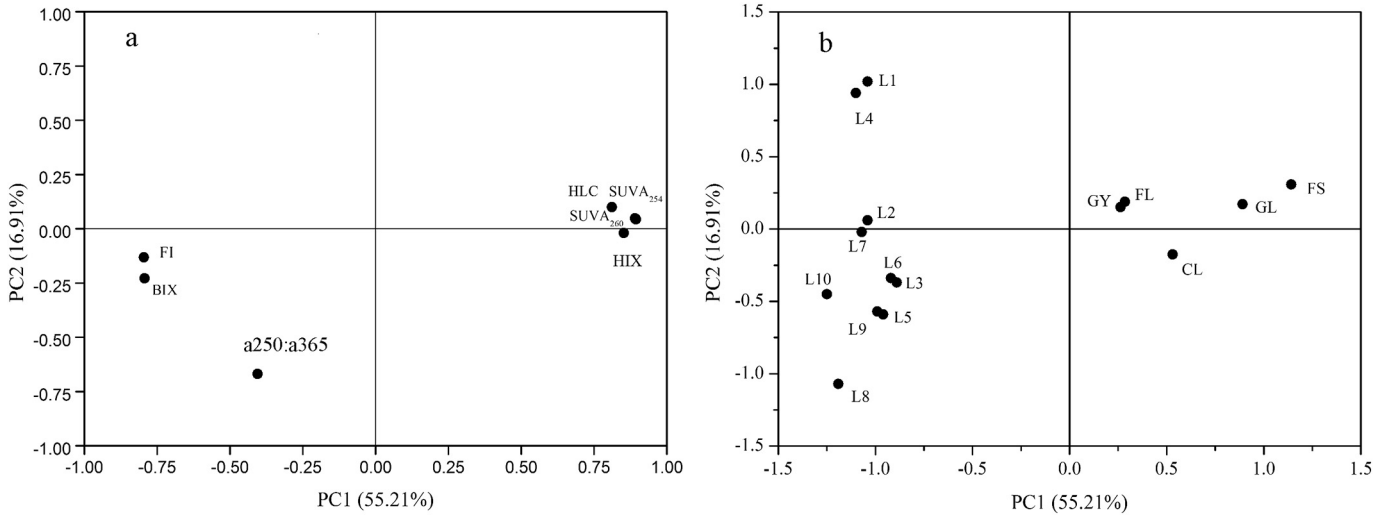

Fig. 8. (a) Factor loading and (b) factor scores plot for the selected DOM characteristics as the first two principal components.

decay byproducts of the organic residues applied to the soil surface of forests. In addition, a greater presence of aromatics, hydrophobic fraction, and molecular size at eroding sites than at depositional sites was observed, thereby indicating that soils with a low amount of condensed polyaromatic structures and a high amount of oxygen-containing functional groups may preferentially be mobilized by soil erosion. But, on the depositional landscapes, continuous input of fresh, presumably more cellulotic organic compounds likely dilutes the concentration of condensed aromatic structures and oxygen-containing functional groups. The DOM in sediments showed an additional protein-like component (tyrosine-like and tryptophan-like combined) in addition to the terrestrial humic-like substances existing in DOM of soils in uplands and gullies, indicating that in deed biological production of organic matter from autochthonous sources could be the primary source of sediment organic matter in the deposition settings. Principal component analysis explained 72% of the variance in the DOM characteristics with the first two principal components and suggested that the DOM in soils made a negligible contribution to DOM in sediments retained by the check dam. Combined results demonstrated that the properties of the sediment DOM at the deposition settings were primarily affected by the autochthonous sources, not allochthonous sources in this study. Further study should take into account the potential variability of solution chemistry and the post-mixing biogeochemical processes for the proper assignments of OM sources and comprehensive investigation of all relevant processes for the fate of SOC at broad spatio-temporal scales from an eco-geomorphologic approach.

Acknowledgments

Financial support for this study came from the “Hundred-talent Project” of the Chinese Academy of Sciences (A315021407), the China Scholarship Fund (201706130055) and the National Natural Science Foundation of China (41271294, 51521006).

References

Assouline, S., Govers, G., Nearing, M.A., 2017. Erosion and lateral surface processes. Vadose Zone J. 16. https://doi.org/10.2136/vzj2017.11.0194.
Bahram, M., Bro, R., Stedmon, C., Afkhami, A., 2006. Handling of Rayleigh and Raman scatter for PARAFAC modeling of fluorescence data using interpolation. J. Chemom. 20, 99–105.
Battin, T.J., Luyssaert, S., Kaplan, L.A., Aufdenkampe, A.K., Richter, A., Tranvik, L.J., 2009. The boundless carbon cycle. Nat. Geosci. 2, 598–600.
Berhe, A.A., Kleber, M., 2013. Erosion, deposition, and the persistence of soil organic matter: mechanistic considerations and problems with terminology. Earth Surf. Process. Landf. 38, 908–912.
Berhe, A.A., Harte, J., Harden, J.W., Torn, M.S., 2007. The significance of the erosion-induced terrestrial carbon sink. Bioscience 57, 337–346.
Berhe, A.A., Harden, J., Torn, M.S., Harte, J., 2008. Role of landform position in erosion-induced terrestrial carbon sequestration. J. Geophys. Res. Biogeosci. 13, G04039. https://doi.org/10.1029/2008JG000751.
Berhe, A.A., Harden, J.W., Torn, M.S., Kleber, M., Burton, S.D., Harte, J., 2012. Persistence of soil organic matter in eroding versus depositional landform positions. J. Geophys. Res. Biogeosci. 117, G02019. https://doi.org/10.1029/2011JG001790.
Berhe, A.A., Barnes, R.T., Six, J., Marín-Spiotta, E., 2018. Role of Soil Erosion in Biogeochemical Cycling of Essential Elements: Carbon, Nitrogen, and Phosphorus. Ann. Rev. Earth Pl. Sc. 46, 521–548.
Bro, R., 1997. PARAFAC. Tutorial and applications. Chemom. Intell. Lab. 38, 149–171.
Cai, Q.G., 2001. Soil erosion and management on the Loess Plateau. J. Geogr. Sci. 11, 53–70.
Carter, M.R., 1993. Soil Sampling and Methods of Analysis. CRC Press.
Chantigny, M.H., 2003. Dissolved and water-extractable organic matter in soils: a review on the influence of land use and management practices. Geoderma 113, 357–380.
Chen, M., Lee, J.-H., Hur, J., 2015. Effects of sampling methods on the quantity and quality of dissolved organic matter in sediment pore waters as revealed by absorption and fluorescence spectroscopy. Environ. Sci. Pollut. Res. 22, 14841–14851.
Chen, F.X., Fang, N.F., Shi, Z.H., 2016. Using biomarkers as fingerprint properties to identify sediment sources in a small catchment. Sci. Total Environ. 557–558, 123–133.
Coble, P.G., 1996. Characterization of marine and terrestrial DOM in seawater using excitation emission matrix spectroscopy. Mar. Chem. 51, 325–346.
Coble, P.G., 2007. Marine optical biogeochemistry: the chemistry of ocean color. Chem. Rev. 107, 402–418.
Coble, P.G., Del Castillo, C.E., Avril, B., 1998. Distribution and optical properties of CDOM in the Arabian Sea during the 1995 Southwest Monsoon. Deep-Sea Res. Part 2 45, 2195–2223.
Cory, R.M., Miller, M.P., McKnight, D.M., Guerard, J.J., Miller, P.L., 2010. Effect of instrument-specific response on the analysis of fulvic acid fluorescence spectra. Limnol. Oceanogr. Methods 8, 67–78.
Derrien, M., Yang, L.Y., Hur, J., 2017. Lipid biomarkers and spectroscopic indices for identifying organic matter sources in aquatic environments: a review. Water Res. 112, 58–71.
Dilling, J., Kaiser, K., 2002. Estimation of the hydrophobic fraction of dissolved organic matter in water samples using UV photometry. Water Res. 36, 5037–5044.
Doetterl, S., Six, J., Wesemael, B., Van Oost, K., 2012. Carbon cycling in eroding landscapes: geomorphic controls on soil organic C pool composition and C stabilization. Glob. Chang. Biol. 18, 2218–2232.
Durrieu, D.E., Madron, X., Abassi, A., Heussner, S., Monaco, A., Aloisi, J.C., Radakovitch, O., Giresse, P., Buscail, R., Kerherve, P., 2000. Particulate matter and organic carbon budgets for the Gulf of Lions (NW Mediterranean). Oceanol. Acta 23, 717–730.
Eilers, K.G., Debenport, S., Anderson, S., Fierer, N., 2012. Digging deeper to find unique microbial communities: the strong effect of depth on the structure of bacterial and archaeal communities in soil. Soil Biol. Biochem. 50, 58–65.
FAO, 2014. World Reference Base for Soil Resources 2014: International Soil Classification System for Naming Soils and Creating Legends for Soil Maps. World Soil Resources Reports 106. Italy, FAO, Rome.
Fernando, L., Rosario-Ortiza, B., Shane, A., Snydera, I.H., 2007. Characterization of dissolved organic matter in drinking water sources impacted by multiple tributaries. Water Res. 41, 4115–4128.
Fissore, C., DalzellB, J., Berhe, A.A., Voegtle, M., Evans, M., Wu, A., 2017. Influence of topography on soil organic carbon dynamics in a Southern California grassland. Catena 149, 140–149.
Fuentes, M., Gonzalez-Gaitano, G., Garcia-Mina, J.M., 2006. The usefulness of UV-visible and fluorescence spectroscopies to study the chemical nature of humic substances from soils and composts. Org. Geochem. 37, 1949–1959.
He, W., Jung, H., Lee, J.H., Hur, J., 2016. Differences in spectroscopic characteristics between dissolved and particulate organic matters in sediments: insight into distribution behavior of sediment organic matter. Sci. Total Environ. 547, 1–8.
Helms, J.R., Stubbins, A., Ritchie, J.D., Minor, E.C., Kieber, D.J., Mopper, K., 2008. Absorption spectral slopes and slope ratios as indicators of molecular weight, source, and photobleaching of chromophoric dissolved organic matter. Limnol. Oceanogr. 53, 955–969.
Huang, M., Li, Z.W., Huang, B., Luo, N.L., Zhang, Q., Zhai, X.Q., Zeng, G.M., 2018. Investigating binding characteristics of cadmium and copper to DOM derived from compost and rice straw using EEM-PARAFAC combined with two-dimensional FTIR correlation analyses. J. Hazard. Mater. 344, 539–548.
Huguet, A., Vacher, L., Relexans, S., Saubusse, S., Froidefond, J.M., Parlanti, E., 2009. Properties of fluorescent dissolved organic matter in the Gironde Estuary. Org. Geochem. 40, 706–719.
Hur, J., 2011. Microbial changes in selected operational descriptors of dissolved organic matters from various sources in a watershed. Water Air Soil Pollut. 215, 465–476.
Jacinthe, P.-A., Lal, R., Kimble, J., 2002. Carbon dioxide evolution in runoff from simulated rainfall on long-term no-till and plowed soils in southwestern Ohio. Soil Tillage Res. 66, 23–33.
Jin, K., Cornelis, W.M., Schiette, W., Lu, J.J., Buysse, T., Baert, G., Wu, H.J., Yao, Y., Cai, D.X., Jin, J.Y., De Neve, S., Hartmann, R., Gabriels, D., 2008. Redistribution and loss of soil organic carbon by overland flow under various soil management practices on the Chinese Loess Plateau. Soil Use Manag. 24, 181–191.
Kaiser, K., Kalbitz, K., 2012. Cycling downwards-dissolved organic matter in soils. Soil Biol. Biochem. 52, 29–32.
Kalbitz, K., Schmerwitz, J., Schwesig, D., Matzner, E., 2003. Biodegradation of soil-derived dissolved organic matter as related to its properties. Geoderma 113, 273–291.
Kirkels, F.M.S.A., Cammeraat, L.H., Kuhn, N.J., 2014. The fate of soil organic carbon upon erosion, transport and deposition in agricultural landscapes-a review of different concepts. Geomorphology 226, 94–105.
Kuzyakov, Y., Cheng, W., 2001. Photosynthesis controls of rhizosphere respiration and organic matter decomposition. Soil Biol. Biochem. 33, 1915–1925.
Lal, R., 1995. Global soil erosion by water and carbon dynamics. Soils Glob. Chang. 131–142.
Lal, R., 2003. Soil erosion and the global carbon budget. Environ. Int. 29, 437–450.
Lal, R., 2004. Soil carbon sequestration to mitigate climate change. Geoderma 123, 1–22.
Lawaetz, A.J., Stedmon, C.A., 2009. Fluorescence intensity calibration using the Raman scatter peak of water. Appl. Spectrosc. 63 (8), 936–940.
Lee, E.K., Chen, V., Fane, A.G., 2008. Natural organic matter (NOM) fouling in low pressure membrane filtration-effect of membranes and operation modes. Desalination 218, 257–270.
Li, Y., Quine, T.A., Yu, H.Q., Govers, G., Six, J., Gong, D.Z., Wang, Z., Zhang, Y.Z., VanOost, K., 2015. Sustained high magnitude erosional forcing generates an organic carbon sink Test and implications in the Loess Plateau, China. Earth Planet. Sci. Lett. 411, 281–289.
Li, Z.W., Liu, C., Dong, Y.T., Chang, X.F., Nie, X.D., Liu, L., Xiao, H.B., Lu, Y.M., Zeng, G.M., 2017. Response of soil organic carbon and nitrogen stocks to soil erosion and land use types in the Loess hilly–gully region of China. Soil Tillage Res. 166, 1–9.
Liu, L., Liu, X., 2010. Sensitivity analysis of soil erosion in the northern Loess Plateau. Procedia Environ Sci 2, 134–148.
Liu, C., Li, Z.W., Dong, Y.T., Chang, X.F., Nie, X.D., Liu, L., Xiao, H.B., Zeng, G.M., 2017a. Do check dam construction and land use change affect a real estimate of soil carbon and nitrogen stocks on the Loess Plateau of China? Ecol. Eng. 101, 220–226.
Liu, C., Li, Z.W., Dong, Y.T., Chang, X.F., Nie, X.D., Liu, L., Xiao, H.B., Wang, D.Y., Peng,

H., 2017b. Response of sedimentary organic matter source to rainfall events using stable carbon and nitrogen isotopes in a typical loess hilly-gully catchment of China. J. Hydrol. 552, 376–386.
Liu, C., Li, Z.W., Chang, X.F., He, J.J., Nie, X.D., Liu, L., Xiao, H.B., Wang, D.Y., Peng, H., Zeng, G.M., 2018a. Soil carbon and nitrogen sources and redistribution as affected by erosion and deposition processes: a case study in a loess hilly-gully catchment, China. Agric. Ecosyst. Environ. 253, 11–22.
Liu, C., Li, Z.W., Chang, X.F., Nie, X.D., Liu, L., Xiao, H.B., Wang, D.Y., Peng, H., Zeng, G.M., 2018b. Apportioning source of erosion-induced organic matter in the hilly-gully region of Loess Plateau in China: insight from lipid biomarker and isotopic signature analysis. Sci. Total Environ. 621, 1310–1319.
Lozovik, P.A., Morozov, A.K., Zobkov, M.B., Dukhovicheva, T.A., Osipova, L.A., 2007. Allochthonous and autochthonous organic matter in surface waters in Karelia. Water Res. 34, 204–216.
Lü, Y.H., Sun, R.H., Fu, B.J., Wang, Y.F., 2012. Carbon retention by check dams: regional scale estimation. Ecol. Eng. 44, 139–146.
Ma, W.M., Li, Z.W., Ding, K.Y., Huang, J.Q., Nie, X.D., Zeng, G.M., Wang, S.G., Liu, G.P., 2014. Effect of soil erosion on dissolved organic carbon redistribution in subtropical red soil under rainfall simulation. Geomorphology 226, 217–225.
McCorkle, E.P., Berhe, A.A., Hunsaker, C.T., et al., 2016. Tracing the source of soil organic matter eroded from temperate forest catchments using carbon and nitrogen isotopes. Chem. Geol. 445, 172–184.
McDowell, W.H., 2003. Dissolved organic matter in soils-future directions and unanswered questions. Geoderma 113, 179–186.
McKnight, D.M., Boyer, E.W., Westerhoff, P.K., Doran, P.T., Kulbe, T., Andersen, D.T., 2001. Spectrofluorometric characterization of dissolved organic matter for indication of precursor organic material and aromaticity. Limnol. Oceanogr. 46 (1), 38–48.
Miao, C.Y., Ni, J.R., Borthwick, A.G.L., 2010. Recent changes of water discharge and sediment load in the Yellow River basin, China. Prog. Phys. Geogr. 34, 541–561.
Murphy, K.R., Butler, K.D., Spencer, R.G.M., Stedmon, C.A., Boehme, J.R., Aiken, G.R., 2010. Measurement of dissolved organic matter fluorescence in aquatic environments: an interlaboratory comparison. Environ. Sci. Technol. 44, 9405–9412.
Murphy, K.R., Stedmon, C.A., Wenig, P., Bro, R., 2014. OpenFluor - an online spectrallibrary of auto-fluorescence by organic compounds in the environment. Anal. Methods 6, 658–661.
Nguyen, H.V., Hur, J., 2011. Tracing the sources of refractory dissolved organic matter in a large artificial lake using multiple analytical tools. Chemosphere 85, 782–789.
Nie, X.D., Li, Z.W., Huang, J.Q., Liu, L., Xiao, H.B., Liu, C., Zeng, G.M., 2018. Thermal stability of organic carbon in soil aggregates as affected by soil erosion and deposition. Soil Tillage Res. 175, 82–90.
Ohno, T., 2002. Fluorescence inner-filtering correction for determining the humification index of dissolved organic matter. Environ. Sci. Technol. 36, 742–746.
Osburn, C.L., Handsel, L.T., Mikan, M.P., Paerl, H.W., Montgomery, M.T., 2012. Fluorescence tracking of dissolved and particulate organic matter quality in a river-dominated estuary. Environ. Sci. Technol. 46, 8628–8636.
Peuravuori, J., Pihlaja, K., 1997. Molecular size distribution and spectroscopic properties of aquatic humic substances. Anal. Chim. Acta 337, 133–149.
Santos, F., Russell, D., Berhe, A.A., 2016. Thermal alteration of water extractable organic matter in climosequence soils from the Sierra Nevada, California. J. Geophys. Res. Biogeosci. 121, 2877–2885.
Shafiquzzaman, M., Ahmed, A.T., Shafiul Azam, M., Razzak, A., Askri, B., Hassan, H.F., Ravikumar, B.N., Okuda, T., 2014. Identification and characterization of dissolved organic matter sources in Kushiro river impacted by a wetland. Ecol. Eng. 70, 459–464.
Smith, S.V., Renwick, W.H., Buddemeier, R.W., Crossland, C.J., 2001. Budgets of soil erosion and deposition for sediments and sedimentary organic carbon across the conterminous United States. Glob. Biogeochem. Cycles 15, 697–707.
Stedmon, C.A., Bro, R., 2008. Characterizing dissolved organic matter fluorescence with parallel factor analysis: a tutorial. Limnol. Oceanogr. Methods 6, 572–579.
Stedmon, C.A., Markager, S., Bro, R., 2003. Tracing dissolved organic matter in aquatic environments using a new approach to fluorescence spectroscopy. Mar. Chem. 82, 239–254.
Sun, W., Shao, Q., Liu, J., Zhai, J., 2014. Assessing the effects of land use and topography on soil erosion on the Loess Plateau in China. Catena 121, 151–163.
Szymański, W., 2017. Quantity and chemistry of water-extractable organic matter in surface horizons of Arctic soils under different types of tundra vegetation – a case study from the Fuglebergsletta coastal plain (SW Spitsbergen). Geoderma 305, 30–39.
Wang, Y.F., Fu, B.J., Chen, L.D., Lü, Y.H., Gao, Y., 2011. Check dam in the Loess Plateau of China: engineering for environmental services and food security. Environ. Sci. Technol. 45, 10,298–10,299.
Wang, L., Shi, Z., Wang, J., Fang, N., Wu, G., Zhang, H., 2014. Rainfall kinetic energy controlling erosion processes and sediment sorting on steep hillslopes: a case study of clay loam soil from the Loess Plateau, China. J. Hydrol. 512, 168–176.
Wang, Z., Guo, S., Sun, Q., 2015. Soil organic carbon sequestration potential of artificial and natural vegetation in the hilly regions of Loess Plateau. Ecol. Eng. 82, 547–554.
Wang, S., Fu, B.J., Piao, S.L., Lv, Y.H., Ciais, P., Feng, X.M., Wang, Y.F., 2016. Reduced sediment transport in the Yellow River due to anthropogenic changes. Nat. Geosci. 9, 38–41.
Weishaar, J.L., Aiken, G.R., Bergamaschi, B.A., Fram, M.S., Fujii, R., Mopper, K., 2003. Evaluation of specific ultraviolet absorbance as an indicator of the chemical composition and reactivity of dissolved organic carbon. Environ. Sci. Technol. 37, 4702–4708.
Wickland, K.P., Neff, J.C., Aiken, G.R., 2007. Dissolved organic carbon in Alaskan boreal forest: sources, chemical characteristics, and biodegradability. Ecosystems 10, 1323–1340.
Wieder, W.R., Cleveland, C.C., Townsend, A.R., 2008. Tropical tree species composition affects the oxidation of dissolved organic matter from litter. Biogeochemistry 88, 127–138.
Xin, Z.B., Qin, Y.B., Yu, X.X., 2016. Spatial variability in soil organic carbon and its influencing factors in a hilly watershed of the Loess Plateau, China. Catena 137, 660–669.
Yang, L., Hur, J., 2014. Critical evaluation of spectroscopic indices for organic matter source tracing via end member mixing analysis based on two contrasting sources. Water Res. 59, 80–89.
Yang, L., Han, D.H., Lee, B.M., Hur, J., 2015. Characterizing treated wastewaters of different industries using clustered fluorescence EEM-PARAFAC and FT-IR spectroscopy: implications for downstream impact and source identification. Chemosphere 127, 222–228.
Zhao, J.L., Van Oos, K., Chen, L.Q., Govers, G., 2016. Moderate topsoil erosion rates constrain the magnitude of the erosion-induced carbon sink and agricultural productivity losses on the Chinese Loess Plateau. Biogeosciences 13, 4735–4750.
Zhou, Y., Shi, K., Zhang, Y., Jeppesen, E., Liu, X., Zhou, Q., Wu, H., Tang, X., Zhu, G., 2017. Fluorescence peak integration ratio IC: IT as a new potential indicator tracing the compositional changes in chromophoric dissolved organic matter. Sci. Total Environ. 574, 1588–1598.
Zsolnay, A., 2003. Dissolved organic matter: artefacts, definitions, and functions. Geoderma 113, 187–209.
Zsolnay, A., Baigar, E., Jimenez, M., Steinweg, B., Saccomandi, F., 1999. Differentiating with fluorescence spectroscopy the sources of dissolved organic matter in soils subjected to drying. Chemosphere 38, 45–50.